2005 International Linear Collider Workshop - Stanford, U.S.A.

First Results with the Prototype Detectors of the Si/W ECAL

D. Strom, R. Frey
University of Oregon, Eugene, OR 97403, USA
M. Breidenbach, J. Deng, D. Freytag, N. Graf, G. Haller
SLAC, Stanford, CA 94025, USA
V. Radeka
BNL, Upton, NY, 11973, USA

Measurements on the prototype silicon sensors for use with an electromagnetic calorimeter with tungsten absorber are reported. The prototype sensors are based on a hexagonal geometry that optimally utilizes the space available on 6 inch silicon wafers. The sensors are segmented into approximately 750 5 mm hexagonal pixels, which are connected to a bump-bonding array located at the center of the sensors. We report on those properties of the sensors that are important for linear collider applications including depletion voltage, stray capacitance and series resistance.

1. INTRODUCTION

Proposed detectors for the International Linear Collider (ILC) are optimized for jet energy reconstruction using the energy flow technique. In this approach, the reconstructed energy and momentum of hadronic jets is based on the momentum of charged particles measured in the tracker, the energy and direction of photons as measured in the electromagnetic calorimeter (ECAL) and the energy and direction of neutral hadrons as measured in the hadronic calorimeter (HCAL). The optimal ECAL will be able to separate the energy of the photons from that of the charged tracks and will allow charged hadrons to be accurately extrapolated into the HCAL so that there will be no double counting of energy.

An attractive technique for an ILC ECAL is a silicon-tungsten sampling calorimeter. Using tungsten as the absorber in the calorimeter keeps the electromagnetic showers compact and avoids confusion of energy from photons with that produced by charged particles. Silicon detectors can be finely segmented and are intrinsically thin allowing for a small gap between tungsten layers that minimizes the size of electromagnetic showers in the detector. This reduces the confusion of charged and neutral energy. For more details on the advantages of the silicon-tungsten approach see Reference [1–5].

In this report we concentrate on the properties of the silicon sensors that are important for the construction of an ILC ECAL silicon-tungsten detector. A primary goal in building the ECAL is to choose a readout technology that allows for a very fine segmentation at a reasonable price. In our design a readout chip is directly bump bounded to each silicon sensor. The granularity of the detector is then determined by the number channels which can be incorporated into a single readout chip[1].

The parameters of the silicon sensors drive the design of the readout chip. The thickness of the depletion layer in the silicon determines the total signal available. The intrinsic and stray capacitance of each pixel determines the noise performance of the system. The series resistance of the traces which connect each pixel to the bump-bonding array is also important. These properties are discussed in Section 2.

Another important property of the silicon sensors are the methods by which they can be tested and calibrated before they are assembled into calorimeter modules. In Section 3 we give examples of possible calibration and testing methods.

---

[1]The design of the readout chip was the subject of a separate presentation [6].

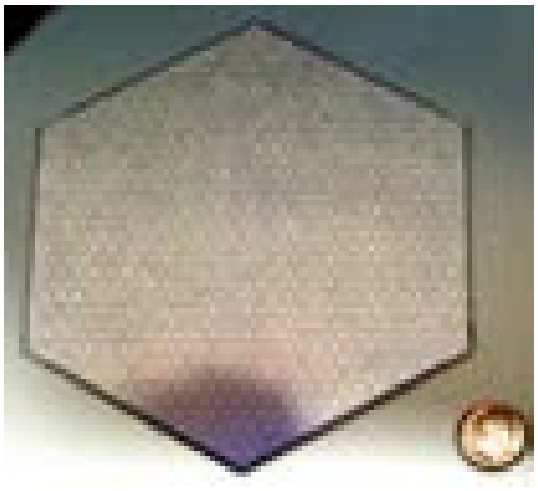

Figure 1: Photograph of a prototype detector. The 5 mm pixels are visible. The bump-bonding array is located in the center of detector.

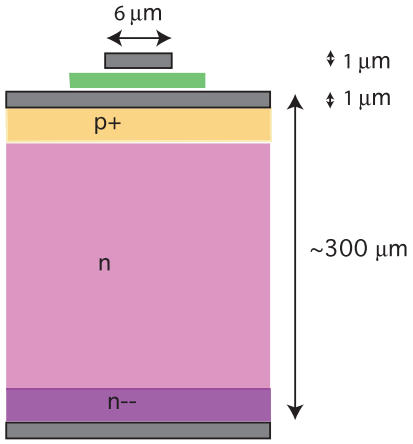

Figure 2: Approximate cross section of the silicon sensors. The diagram shows one of the traces which connects the pixels to the bump-bonding array located in the center of the detector.

2. SILICON SENSOR PROPERTIES

The measurements reported here are based on one of ten detector prototypes which were manufactured by Hamamatsu to our specifications. The detectors are based on the largest hexagon which could be inscribed into the active area of a 6 inch silicon wafer. The wafers were subdivided into hexagonal pixels of 5 mm, giving a total of 757 pixels. The detectors are approximately 300 μm thick. A photograph of the detector is shown in Figure 1. The approximate cross section of the detector, including a sample trace which connects a pixel to the bump-bonding array is shown in Figure 2.

2.1. Detector Signals

The expected size of a signal in a silicon detector depends on the total thickness of the depleted region in the detector. For a depletion region of 300 μm we expect a minimum ionizing particle (MIP) to create approximately 24,000 electron hole pairs in the silicon. In Figure 3 we show the signal due to cosmic ray muons that were measured in one of the prototypes detectors. For the test, a single pixel of the detector was readout with a probe attached with a coax cable to a commercial AMPTEK A250F charge amplifier. The output of the AMPTEK was shaped and digitized in a manner similar to that expected to be implemented in the ILC readout electronics. For the data shown in the figure, the system was triggered by a second silicon detector with 1 cm square pads located approximately 1 cm below the detectors under test. The detector was biased with 80 V. The collected charge as function of bias voltage is shown in Figure 4.

For the laboratory electronics used, the total noise was approximately 800 electronics. This gives a signal-to-noise ratio of approximately 30. In the actual detector we can tolerate a much worse signal-to-noise, and the area and power consumption of the readout chip can be reduced if we allow a signal-noise-ratio as poor as 12. Since we can obtain reasonable signal-to-noise with 300 μm thick detectors there is no reason to consider thicker detectors. A possible disadvantage of a thicker detector is that they have increased maximum charge. For example, a 500 GeV electromagnetic shower is expected to have some pixels with a charge signal corresponding to 2000MIPs or more. In a 300 μm thick silicon sensor, this corresponds to a charge of almost 8 pC that must ultimately be stored on the feedback capacitor of the charge amplifier. This requires a feedback capacitor of at least 10 pF to keep the voltages

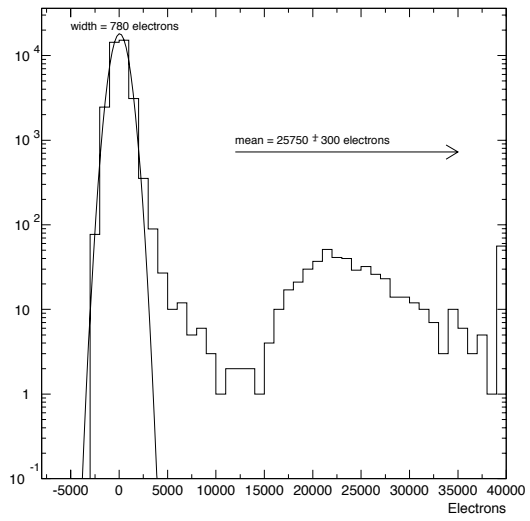

Figure 3: Measured distribution of charge for cosmic ray tracks. The error on mean does not include a $\sim 10\%$ calibration uncertainty. The last bin shows overflows.

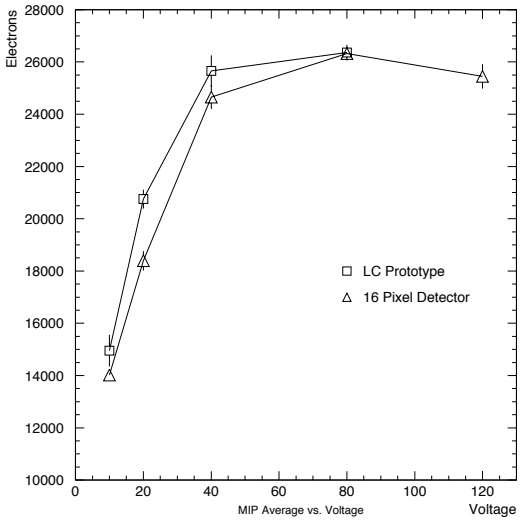

Figure 4: Measured mean charge as function of bias voltage for the new prototypes and an older detector of similar construction. The errors are statistical only and do not include a $\sim 10\%$ calibration uncertainty.

below 1 V so that a low voltage CMOS process can be used for the production of the readout chip. If the detector thickness were doubled, it would be necessary to use an even larger feedback capacitor, driving up the area of the readout chip.

2.2. Pixel Capacitance and Trace Resistance

In almost all cases the noise of an individual pixel charge measurement in our detector will be directly proportional to the total capacitance seen at the input of the amplifier. The capacitance of a fully depleted 5 mm pixel is expected to be approximately 5.7 pF. The majority of the capacitance is due to the stray capacitance of the traces which connect the individual pixels to the bump-bonding array.

For the Hamamatsu process used in our detectors, the thickness of the oxide to the second metal layer is approximately $0.9\,\mu$m. In our detector we used $6\,\mu$m thick traces, giving a theoretical capacitance of approximately 3.1 pF/cm [7]. The total amount of stray capacitance associated with a given pixel has two contributions. One contribution comes from the capacitance of the traces connecting the pixel to the bump-bonding array. The second contribution is due to any traces from other pixels which cross the pixel under test. The total stray capacitance is almost constant for many of the pixels as can be seen from Figure 5. In regions a and b it can be seen that pixels located closer to the bump-bonding array have a greater number of crossing traces than those further away. This gives an almost constant total measured (and calculated) stray capacitance. Typical stray capacitances in region a were ~ 22 pF. An example run is shown in Figure 6.

A small fraction of the pixels have a very large number of crossing traces. These pixels are located in region d of Figure 5. For the first prototypes these pixels have capacitances of somewhat more than 100 pF. In a future version of the sensors we plan to reduce the stray capacitance by narrowing the traces in the vicinity of the bump-bonding array.

Another important property of the detectors is series resistance of the traces. The noise contribution from this series resistance is proportional to $C_{tot}\sqrt{R_s}$ where C_{tot} is the total input capacitance and R_s is the series resistance. The contribution to the noise from the input FET in a charge amplifier is proportional to $C_{tot}\sqrt{\frac{2}{3g_m}}$ where g_m is the transconductance of the input FET. Thus it is desirable to keep R_s comparable to $\frac{2}{3g_m}$. In our case we expect $\frac{2}{3g_m} \sim 300\,\Omega$.

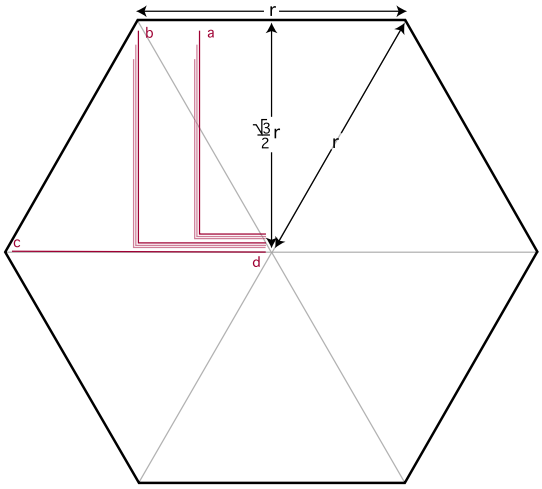

Figure 5: Example traces with varying amounts of stray capacitance. In the prototypes the $r = 6.75\,\mathrm{cm}$.

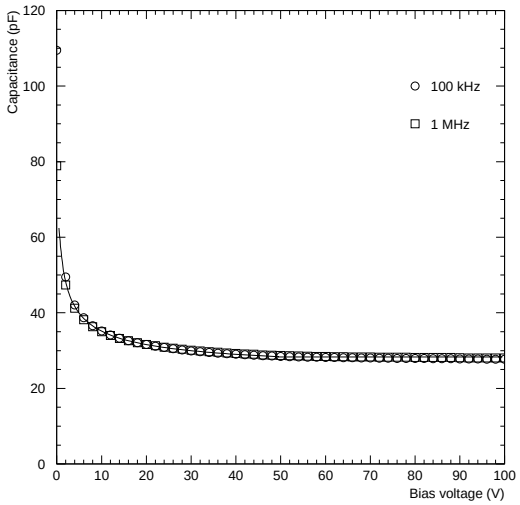

Figure 6: Typical capacitance versus bias voltage curve for a pixel located near region a.

Based on the measurement of one of the trace's resistance, we obtain a trace resistance of $57 \pm 2\Omega$/cm. This can be compared to an expected value of 47Ω/cm for a pure aluminum traces 1μm by 6 μm. For the longest traces, of order 10 cm, the measured value implies a maximum resistance of $570\,\Omega$.

It would be desirable to reduce this trace resistance by making thicker traces, however, it is unlikely that the thickness can be increased much beyond its current value of $1\,\mu$m. Increasing the width of the trace is not helpful because it will increase the component of C_{tot} from the traces connecting the pixels to the bump-bonding array almost linearly. Except in the region near bump-bonding array, our trace width of 6 μm is close to optimal.

2.3. Leakage Current

Leakage current can add an additional term to the electronic noise that grows with shaping time. Typical leakage currents in silicon pad detectors such as the prototypes used here give currents of a few nA/cm^2. The leakage current was measured during the capacitance tests and was found to be less than 2 nA/pixel for pixels in the interior of the detector. In our tests the neighboring pixels and the guard ring were left "floating" . For pixels on the edge of the detector, with the guard ring floating, the leakage current was less than 10 nA/pixel. We expect the noise contribution for leakage current to be minimal; the expected contribution for a leakage current of 10 nA and an integration time of $1\,\mu$s is only 250 electrons.

3. CALIBRATION

Calorimeters based on silicon are expected to be quite stable over time. The largest changes in calorimeter response will be due to changes in the electronics. The readout electronics are being designed with an internal calibration system that allows a wide variety of charges to be injected into each of the channels in the system. The accuracy of this system is expected to be limited by the knowledge of the values of the coupling capacitors incorporated into each of the channels in the readout chip. These capacitors are expected to be uniform, within a chip, with a spread of $\sim 1\%$. This spread is unlikely to have a noticeable contribution to the energy resolution of the calorimeter. Chip-to-chip variations could be larger.

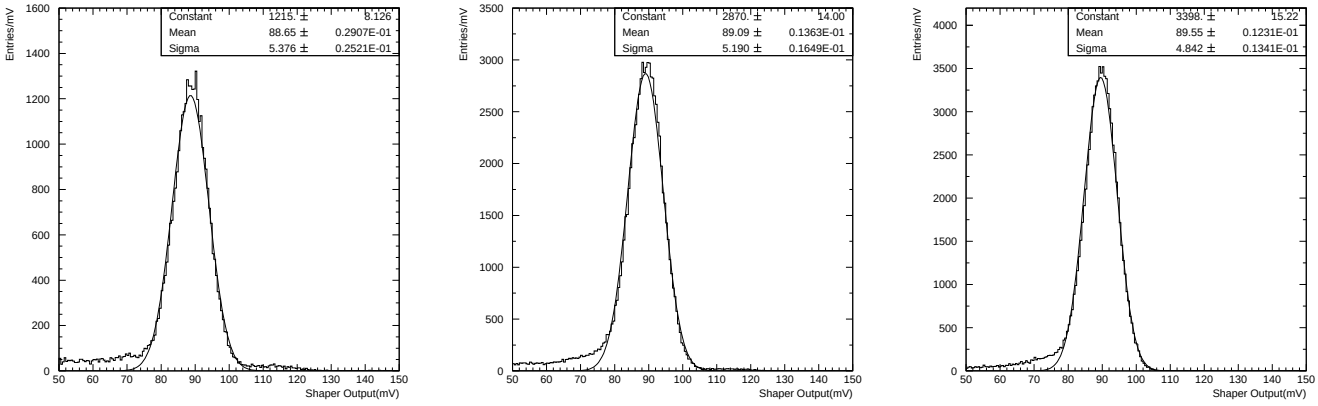

Figure 7: Signals from Am^{241} 60 keV photons observed in the Hamamatsu silicon sensors in 3 different pixels.

One possibility is to calibrate each sensor after the readout chip has been bump bonded. A possible method for this calibration would be to use 60 keV photons from the decay of radioactive Am^{241}. If the energy from these photons are fully contained in the silicon sensors they will give a signal of approximately 16,000 electrons. This is somewhat less than the MIP signal, but well above our noise floor.

The 60 keV photons will easily penetrate any mounting structures and printed circuit boards used in the testing and assembly of the calorimeter. However, the calibration must be done before the detector assemblies are placed between the tungsten sheets, as the photons will not efficiently penetrate the tungsten. We have used our laboratory electronics to measure the energy spectrum from the Am^{241} photons in a few pixels as shown in Figure 7. The widths of the peaks are consistent with the expected electronic noise.

In the readout chip planned for the final detector, the signal-to-noise for Am^{241} peak will be about 8, which will broaden the peak considerably. Another important aspect of the planned readout electronics will be that a measurement of the charge will be done relative to an external bunch clock rather than relative to the time of arrival of the photon as was done in the laboratory. This will lead an additional smearing of the observed spectrum of less than 5%. Thus we expect a total width for the Am^{241} 60keV signal of approximately 15%.

The ADC in the planned detector readout will have a least significant bit approximately equal to the expected noise. Therefore, if there were no systematics in the ADC it would be possible to calibrate each pixel to 1% with approximately 250 detected photons. For this calibration to be useful it will be necessary to relate the charge scale at 8 ADC counts to that at full scale readout. This is possible, but will require great care in the design of the calibration circuit on the readout chip.

Somewhat easier, but still difficult, will be a wafer to wafer calibration at the sub-percent level. Here one can average over 1024 pixels/wafer. Again it will be necessary to relate the average charge scale at 8 ADC counts to the average full scale readout.

Another probe of the silicon sensors are nanosecond infrared laser pulses which are focused to a 10μm diameter spot using a microscope. Some of the pixels in the Hamamatsu sensors have been equipped with small windows in the metallization that allow the laser pulses to penetrate the active area of the silicon detectors. In our setup we use 1064 nm light so that electron-hole pairs will be created throughout the active volume of silicon and not be absorbed at the silicon surface as would be the case for visible light. The response of laboratory setup to these pulses are shown in Figure 8. Note that the nonlinear response and the discontinuity between the 6 ns and 20 ns pulse widths is a property of our ability to control the laser rather than an indication of a nonlinear response of the silicon.

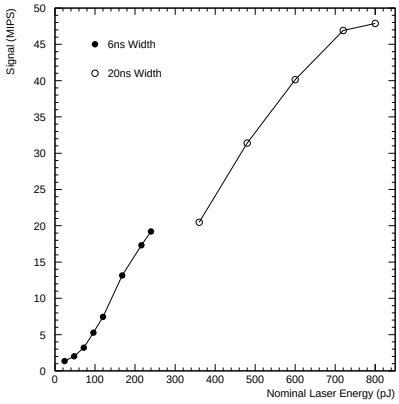

Figure 8: Signals from short laser pulses of 1064 nm light as a function of nominal laser energy.

4. CONCLUSION

We have tested a prototype silicon sensor and find that it has adequate properties for use in an ILC ECAL. In future versions of the silicon sensors we will attempt to reduce the stray capacitance by narrowing traces connecting the pixels to the bump-bonding array in the vicinity of the bump-bonding array. We will also increase the number of pixels to 1024 and attempt to optimize the trace layouts to reduce stray capacitance and series resistance. We have also shown that cosmic rays, radioactive sources and infrared lasers can be used to characterize the detectors. These probes will be useful in the future to test the detectors after the readout chip has been attached to the detector.

Acknowledgments

The authors wish to thank the organizers for hosting a well run workshop. We also wish to thank T. Neely and E. Fitzgerald for assisting in making some of the measurements reported here. This work is supported by U.S. Department of Energy.

References

[1] J. Brau, A. Arodzero, D. Strom, "Calorimetry for the NLC Detector," in *Proc. of the 1996 DPF/DPB Summer Study on New Directions in High-energy Physics*, SLAC-PUB-7693.

[2] H. Videau and J. C. Brient, "A Si-W calorimeter for linear collider physics," in *Proc. 10th International Conference on Calorimetry in High Energy Physics (CALOR 2002)*, Pasadena, California, 25-30 March 2002, pp. 309-320.

[3] D. Strom, R. Frey, M. Breidenbach, D. Freytag, N. Graf, G. Haller, O. Milgrome, V. Radeka, "Design and development of a dense, fine grained silicon tungsten calorimeter with integrated electronics," CALOR04 March, 2004, Perugia, Italy.

[4] R. Frey, D. Strom, M. Breidenbach, D. Freytag, N. Graf, G. Haller, O. Milgrome, V. Radeka, "Silicon/tungsten ECal for SiD - Status and Progress," LCWS04, April 2004 , Paris, France.

[5] D. Strom, R. Frey, M. Breidenbach, D. Freytag, N. Graf, G. Haller, O. Milgrome, V. Radeka, "Fine Grained Silicon-Tungsten Calorimetry for a Linear Collider Detector", NSS-MIC November 2004, Rome, ITALY.

[6] M. Breidenbach, "Design Consideration for Si/W ECAL Electronics," LCWS05, Stanford, CA, March, 2005.

[7] F.E. Borgnis and C.H. Papas, "Electromagnetic Waveguides and Resonators", Handbuch der Physik 16, 377 (1958).